ELSEVIER

Materials Science and Engineering A208 (1996) 172–180

MATERIALS SCIENCE & ENGINEERING A

Effect of composition on crystallographic texture in hot-rolled Al–Li–Cu alloys

A.K. Vasudévan[a], M.A. Przystupa[b], W.G. Fricke Jr.[c,1]

[a]*Office of Naval Research, Code-332, 800 N. Quincy St., Arlington, VA 22217, USA*
[b]*Department of Materials Science and Engineering, University of California, Los Angeles, CA 90024, USA*
[c]*Alcoa Technical Center, Alcoa Center, PA 15069, USA*

Received 8 September 1995

Abstract

The hot-rolling textures of ternary Al–Li–Cu alloys have been characterized to determine their effects on the yield strength anisotropy. The alloys used in the study had (Li/Cu) ratios varying from 0 to ∞ and were hot-rolled in the 520–400 °C temperature range. All the alloys showed well developed β-fibers, with a maximum intensity at Brass, and a weak background of α-fiber. The Brass components were very strong for the alloys with intermediate (Li/Cu) ratios that had relatively more T_1 precipitates in the microstructure compared with other alloys. In addition, all compositions showed a weak Cube or rotated Cube recrystallization texture components. The observed textures are attributed to the effects of constrained deformation during hot deformation. The texture results were used to predict the yield strength anisotropies in the alloys. The predictions were in agreement with the experimental results for the high (Li/Cu) alloys. However, in the low (Li/Cu) alloys, the discrepancies between the predicted and the measured yield strength anisotropies can be attributed to a modifying effect of the directional platelet precipitates on deformation.

Keywords: Hot-rolling textures; Anisotropy

1. Introduction

The wrought Al–Li–Cu–(Mg) alloys have been known to have unusually high yield strength anisotropy [1–3]. The source of this anisotropy has been mainly attributed to the crystallographic texture and, in particular, to the strong Brass texture component. To date, most of the quantitative texture studies on the heat-treatable Al–Li alloys have been devoted to the development of cold rolling textures in the presence of a stable precipitation structure [4,5]. In contrast, during hot rolling both precipitation and dynamic recrystallization can occur simultaneously, affecting the outcome of the final texture. In the non-heat-treatable aluminum alloys, where dynamic precipitation is minimal or absent, the effects of recrystallization on the hot-rolling texture have been well documented [6–9]. In an earlier paper, we have addressed the role of the precipitation of δ-phase on the hot rolling texture development in the Al–Li binary alloys [10]. It was observed that increasing Li content increased the volume fraction of δ at high temperatures, thereby suppressing the dynamic recrystallization and homogenizing the texture. The hot-rolling textures of the Al–Li binary alloys showed distinct β-fibers with a maximum intensity between Brass and Goss at $(\bar{1}01)[1\bar{4}1]$.

In this paper, we extend the binary Al–Li alloy discussions to the development of hot-rolling textures in a series of ternary Al–Li–Cu alloys. The compositions of these alloys have been selected at the maximum solubility limit, allowing each alloy to develop different combination of the dynamically precipitating phases. These phases include matrix δ', {100} habit plane Θ and T_b, {111} habit plane T_1 and grain boundary δ and rod shape T_2 precipitates.

[1] Deceased.

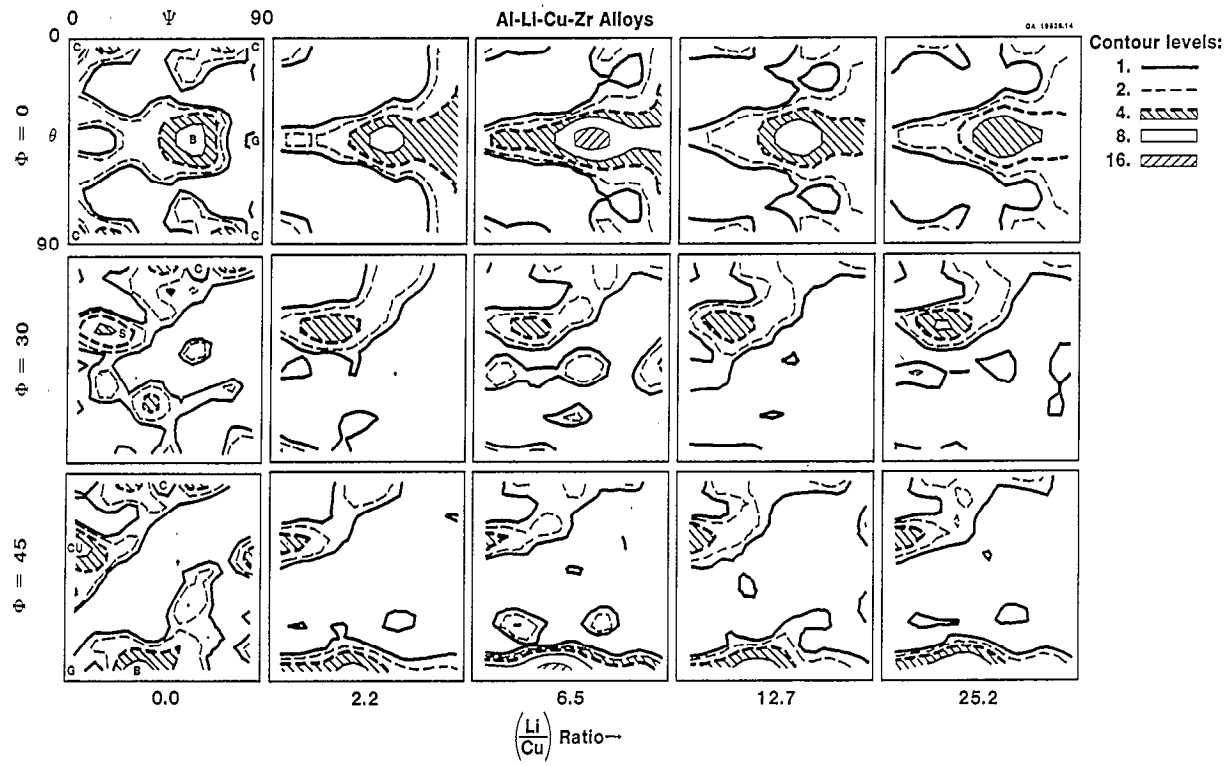

Fig. 1. ODF $\phi = 0°$, 30°, and 45° sections for the Al–Li–Cu alloys with increasing (Li/Cu) ratios. Major texture components have been marked as B = Brass, Cu = Copper, C = Cube, G = Goss and S.

2. Experimental procedures

2.1. Materials and processing

The chemical composition of the six experimental alloys used in this investigation are listed in Table 1. Alloys M and R are binary alloys, while the remaining four alloys have both Li and Cu contents adjusted to give (Li/Cu) ratios varying from 2.2 to 25.2. These particular compositions were chosen at the limits of the ternary solid solubility at 516 °C [11]. All the alloys contained 0.11 to 0.17 wt.% Zr, intentionally added to suppress recrystallization. The alloys were fabricated from 254 mm thick ingots, scalped, preheated for 8 h at 520 °C and hot-rolled. The average temperature of the ingots at the start of hot-rolling was about 520 °C. The exit temperature was around 400 °C. The final thickness of all plates was 12.7 mm. After rolling the alloys were solutionized, cold water quenched and aged to give peak strength. The yield strengths of all the alloys were measured along 0° and 45° orientations with respect to the rolling direction.

2.2. Texture characterizations

The X-ray texture samples were cut from the plate mid-sections, with test planes parallel to the rolling plane. For every alloy complete (111) and (200) polefigures were measured by combining the partial polefigures obtained in the transmission and reflection modes. This gave results that did not contain errors from the approximation of textures in the unknown regions commonly associated with only one measurement. The (111) and (200) polefigure data were subsequently used in calculating the ODF intensity maps using Roe's spherical harmonic method [12].

3. Texture results

The ODF results, in Roe's Euler angles ϕ, ψ and θ, are summarized in Fig. 1. Only sections with $\phi = 0°$, 30° and 45° have been shown, because they contain the major texture components. These components are marked in Fig. 1 and they include Cube (C) on all sections, Goss (G) and Brass (B) on sections $\phi = 0°$ and 45°, S at $\phi = 30°$ and Cu–Taylor/Dillamore (Cu) components on section $\phi = 45°$. The ODF results for different alloys have been grouped in columns and are shown with intensity contours at 1, 2, 4, 8 and 16 times random. Fig. 2 also shows the texture evolution with composition on the ternary Al–Li–Cu phase diagram with ODF $\phi = 0°$ sections.

The salient features of textures in Fig. 1 are α- and β-fibers and weak recrystallization components. The strongest ODF intensities were along the β-fibers; they form high intensity tubes extending from $\phi = 0°$ to $\phi = 45°$ with Brass and Cu–Taylor/Dillamore components at the respective ends. The α-fibers were always confined to the section $\phi = 0°$ appearing as high intensity ridges along $\theta = 45°$. We also observed the following common characteristics in texture among all the alloys:

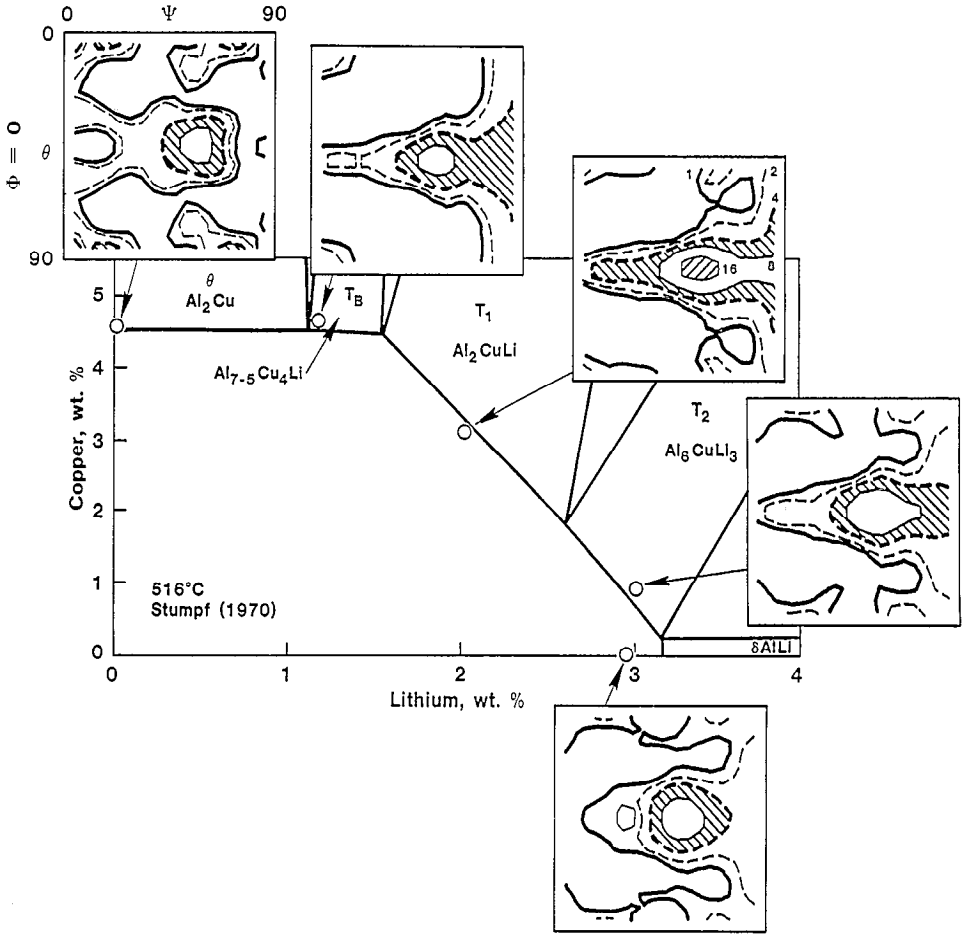

Fig. 2. Ternary Al–Li–Cu phase diagram, at 516 °C, with superimposed $\phi = 0°$ ODF's for the indicated alloys.

- The α-fibers, Fig. 3, had maxima at Brass, $\psi = 54.6°$, with relatively constant background intensity away from the peak. The background intensities were always higher at $\psi = 90°$ (that is at the Goss location), than at $\psi = 0°$. Similar textures have been reported in other hot-rolled fcc alloys [13]. This type of texture is commonly referred to as the "hot-rolling deformation texture".
- The Brass and Goss components, Fig. 4, had maximum intensities for alloy O (Li/Cu ratio equal 6.5). For other ternary alloys these intensities were nearly

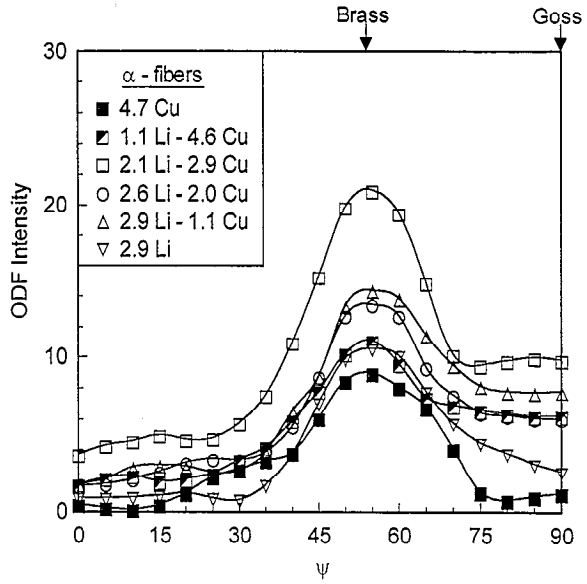

Fig. 3. ODF texture intensities along α-fibers for the hot-rolled Al–Li–Cu alloys. In all cases $\phi = 0°$ and $\Theta = 45°$.

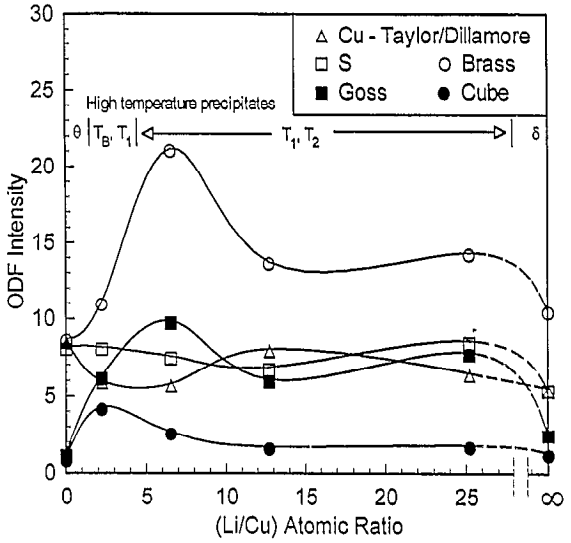

Fig. 4. ODF intensities of the major texture components vs. (Li/Cu) ratio. Volume fraction of T_1 and T_2 is decreasing when (Li/Cu) > 6.

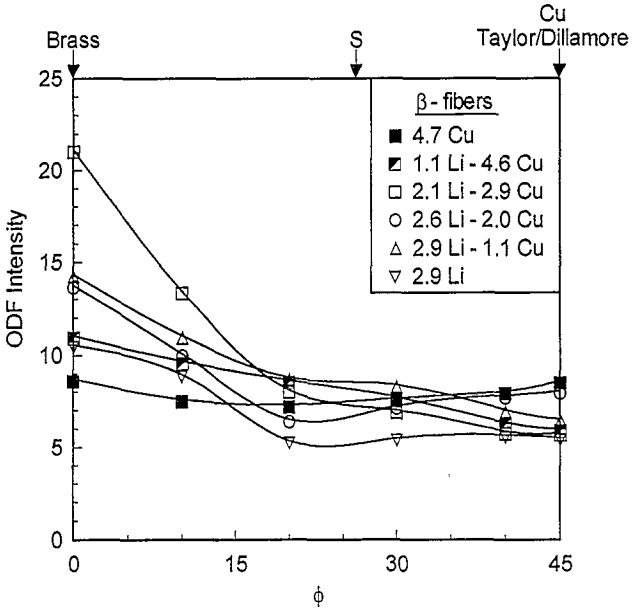

Fig. 5. ODF texture intensities along β-fibers for the Al–Li–Cu alloys.

the same and for the binary Al–Cu and Al–Li alloys they were the weakest. The strongest Brass, 21.2 times-random, was in alloy O. Binary Al–Cu alloy had the weakest Brass which was only 8.72 times random.

- The intensities along the β-fibers decreased with increasing ϕ angle, Fig. 5. This decrease was monotonic for the ternary alloys N, O and Q. Both binaries and ternary alloy P had a local minima near the S texture component. The intensities for all β-fibers at $\phi = 45°$ section were very similar, varying between 6° and 9°.
- The position of the β-fibers did not change significantly with alloy composition, Fig. 6. For the binary Al–Cu alloy β-fiber extended from $\phi = 0°$, $\theta = 45°$ and $\psi = 54.6°$, corresponding to an ideal Brass position, and terminated at $\phi = 45°$, $\theta = 30.8°$ and $\psi = 0°$, which is 3.6° away from the Taylor/Dillamore and 4.5° from the Cu component. With increasing (Li/Cu) ratio the starting position of the β-fiber moved only about 2° away from the Brass to the higher ψ angles. At the same time, the end of the β-fiber shifted by about 3° towards lower θ angles, that is near ideal Taylor/Dillamore position.
- All recrystallization texture components were relatively weak with the Cube component less than two times random. The two exceptions were in the alloys N and O, with (Li/Cu) ratios 2.2 and 6.5, which had Cube intensities 4.3 and 2.7 respectively. Rotated Cube components were observed located either at (001)[130] for the binary Al–Cu (alloy M) and at (001)[120] for ternary alloys (P and Q). The presence of these rotated Cube components may be associated with some degree of particle stimulated recrystallization [5]. This observation has been supported by previous optical microscopy study that showed small area fraction of recrystallized grains in these alloys [14].

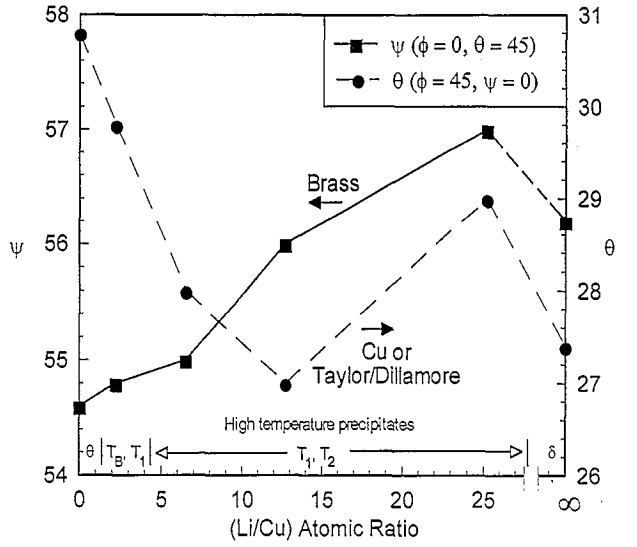

Fig. 6. Positions of the Brass (■ – $\phi = 0°$, $\Theta = 45°$) and Cu–Taylor/Dillamore (● – $\phi = 45°$, $\psi = 0°$) ends of β-fiber vs. (Li/Cu) ratio. Volume fraction of T_1 and T_2 is decreasing when (Li/Cu) > 6

4. Discussion

An important trend observed in the hot-rolling textures of the ternary Al–Li–Cu alloys was an initial increase, followed by a decrease in the Brass component intensity with increasing (Li/Cu) ratio. To understand this trend, it is necessary to examine the changes in the precipitation sequences occurring during hot working.

The possible equilibrium phases present in the Al–Li–Cu alloys after hot-rolling are indicated on the ternary phase diagram at 516 °C solvus in Fig. 2 [11,14]. These high temperature phases precipitate out when the alloy temperature cross their respective phase fields. According to Fig. 2 there are five possible equilibrium precipitates that can form by varying the (Li/Cu) ratio. Considering their shapes and habit planes, they can be divided into three groups. The first group includes precipitates which are platelets with {100} habit planes. These are Θ and T_B phases. The T_1 platelets with {111} habit planes constitute the second group. The last group includes T_2 and δ precipitates which do not have preferential habit planes and can form both in the matrix and on the grain boundaries. Given favorable kinetics during hot rolling, the alloys can have more than one type of precipitate forming simultaneously, or in sequence. The equilibrium phases that have been reported in the Al–Li–Cu alloys after rolling are listed in the last colum in Table 1 [11,14–17]. At the hot rolling temperatures, these precipitates can

Table 1
List of alloy compositions and their corresponding precipitates

Alloy designation	(Li/Cu) atomic ratio	Li wt.%	Cu wt.%	Zr wt.%	Precipitates/habit plane/shape at temp. 300 to 516 °C
M	0	–	4.7	0.12	Θ/{100}/platelets
N	2.2	1.1	4.6	0.17	T_B/{100}/platelets T_1/{111}/platelets
O	6.5	2.1	2.9	0.12	T_1/{111}/platelets T_2/{100}/platelets[a]
P	12.7	2.6	2.0	0.13	T_1.{111}/platelets T_2/{100}/platelets[a]
Q	25.2	2.9	1.1	0.11	T_1/{111}/platelets T_2/{100}/platelets[a]
R	∞	2.9	–	0.11	δ/particles[a]

Fe = 0.06, Si = 0.04, Ti = 0.01
[a] Matrix and/or grain boundary precipitates, depending on temperature.

be coarse in size compared with the ones formed at the lower aging temperatures. To date, there seems to be a lack of a systematic documentation on the elevated temperature microstructures in these alloys.

The effect of course precipitates and/or particles on the development of hot-rolling texture in aluminum alloys have been studied by only a few investigators. A detailed work on the subject has been conducted for the Al–Fe–Si alloys containing low and high volume fractions of iron particles [6]. The alloys showed an increase in the Brass texture intensity when the hot rolling temperature was increased from 200 to 300 °C. However, the maximum intensity along the β-fiber was at Cu for an alloy with low particle volume fraction and at S for alloy with high particle content. When the same alloys were cold rolled, the textures were weaker with maximum at Cu and a very weak Brass component for both alloys. Similar studies on the 8090 alloy (2.58Li–1.24Cu–0.7Mg–0.12Zr) showed that hot rolling resulted in the development of β-fiber with a peak intensity at Cu [18]. Cold rolling gave β-fiber with maximum at S and minimum at Brass. The Brass component had similar intensities for both hot and cold rolling. In contrast, the binary Al–Li alloys showed a shift in the hot-rolling textures from the Goss-type to the β-fiber type with increasing Li content [19,10]. The maximum intensity was observed at Goss for low Li alloys and at Brass when the Li content exceeded 2 wt.%. These changes were attributed to the precipitation δ-phase during rolling [10].

Effects of precipitation on the development of cold rolling textures in the fcc alloys have been well documented [4,5,20]. Results suggest that the precipitation state prior to rolling strongly affects the deformation pattern, hence also the final texture. In the supersaturated solid solution alloys, and for low rolling reductions, the deformation is homogeneous, resulting in the development of Cu and S textures. Increased rolling reductions trigger shear bands within the grains, giving rise to an increase in the Goss and Brass texture intensities. These types of textures and deformation patterns have been observed in the alloys which were initially in the underaged conditions and had low volume fractions of shearable precipitates. With increasing volume fraction of these precipitates, the shear bands became macroscopic, overall texture intensity weakened and the Brass intensity increased. In the overaged conditions, with particles being non-shearable, deformation becomes homogeneous decreasing the average texture intensity and shifting the peak intensity from Brass to Cu. Finally, for the severely overaged conditions and/or higher volume fraction of coarse non-sharable particles, the cold rolling results in the formation of the highly deformed zones surrounding the particles which randomize the final texture.

Based on the above results of texture–precipitate interactions for the cold-rolling, one can expect similar behavior during hot-rolling of the Al–Li–Cu alloys. The dynamics in the hot-rolling case are however more complex because: (1) precipitate form and grow during rolling; (2) they can have different shapes and orientations depending on the (Li/Cu) ratio, and (3) dynamic recovery and recrystallization can be taking place simultaneously with dynamic precipitation. Comparing the composition ranges for the presence of different types of precipitates with texture (Figs. 2 and 3), it appears that increase in the intensity of Brass component coincides with the dominance of T_1 in the microstructure. Since T_1 is the only {111} habit plane precipitate in the Al–Li–Cu system, it can have a modifying effect on texture that may be different from the other types of precipitates. It has been reported recently that the alloys with compositions corresponding to peak Brass intensity seem to show serrated yielding during superplastic forming at 500 °C [21]. This can suggest strong solute-dislocation interactions which could result in the development of shear bands.

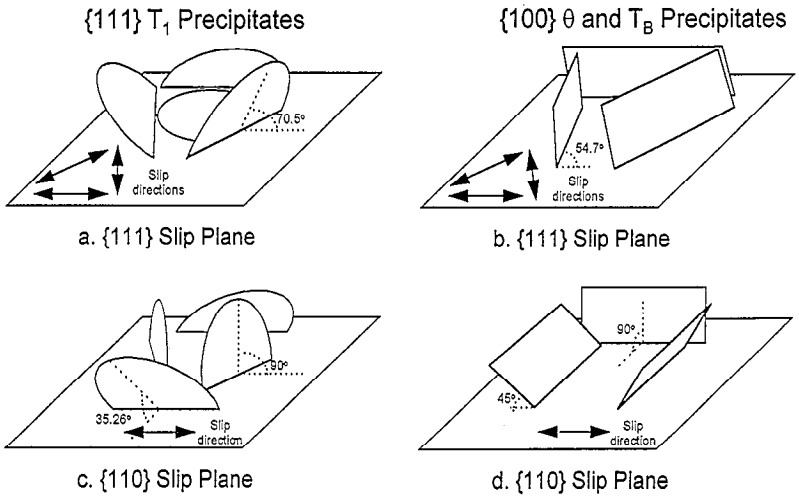

Fig. 7. Schematic illustrations showing the {111} and {100} habit plane precipitates intersecting the {111} and {110} slip planes.

To analyze the effects of different precipitates in the Al–Li–Cu alloys on slip, we consider their spacial arrangements with respect to the potential slip planes. In aluminum alloys, the primary slip takes place on the octahedral {111} planes and along ⟨110⟩ directions both at high and low temperature deformations. It has been shown that above 0.6 homologous temperatures, the slip can also occur on the non-octahedral {110} planes and along ⟨110⟩ directions [22]. For a {111} slip, one variant of T_1 precipitate lie on the slip plane and the remaining three intersect the slip plane at 70.5°, Fig. 7(a). For the {100} Θ platelets-like and T_B precipitates, all three variants intersect the {111} slip plane at 54.7°, Fig. 7(b). In the case of non-octahedral {110} slip, two of the T_1 variants are perpendicular to the slip planes and two intersect them at 35.26°, Fig. 7(c). Similarly, one of the three variants of the Θ and T_B will be perpendicular to the {110} slip plane and the remaining two will intersect the {110} at 45 °, Fig. 7(d). Such directional precipitates can then result in different critical resolved shear stresses on the {111} and {110} planes. The ratios of these stresses, considering only the precipitation strengthening components, can be estimated by assuming that:

(1) τ_{crss} is proportional to the square root of the planar obstacle densities, N_a, [18,23]

$$\tau \propto F\frac{\sqrt{N_a}}{b}$$

where F is obstacle strength and b the Burgers' vector;

(2) obstacle densities are proportional to the probabilities, P, of intersecting a given precipitate variant with the slip plane [24]

$$N_a \propto P$$

Expressing the probabilities by the sine of the angle between the precipitate variants and the slip planes [24], one can calculate the ratio of the precipitate shear stress components on the {111} and {110} slip planes. For the {111} habit plane precipitates this ratio is:

$$\left(\frac{\tau_{\{111\}}}{\tau_{\{110\}}}\right)_{\{111\}ppt} = 0.947$$

while for the {100} precipitates it is equal to:

$$\left(\frac{\tau_{\{111\}}}{\tau_{\{110\}}}\right)_{\{100\}ppt} = 1.131$$

Although these estimations do not include the yield strength components from the intrinsic lattice resistance of the matrix, their values indicate that during hot-rolling of the Al–Li–Cu alloys, the non-octahedral slip can be more active in the presence of the {100} rather than {111} precipitates. This could mean that the non-octahedral slip is not responsible for the development of strong Brass texture components in these hot-rolled alloys because the Brass peak intensity coincides with the higher volume fraction of T_1 precipitates, Fig. 3.

If one can assume octahedral slip, then the likely source of the strong Brass in the Al–Li–Cu ternary alloys can be the presence of B-type shears during

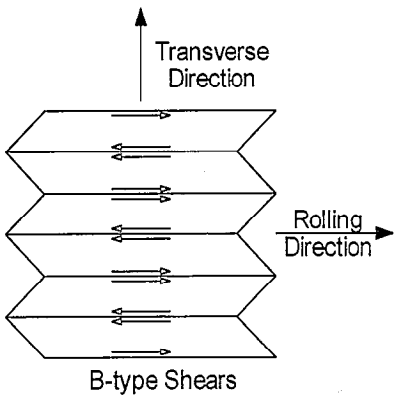

Fig. 8. Illustration of microscopic B-shear pairs in the neighboring grains or, alternatively, between various regions within one grain.

rolling [25–27], Fig. 8. These shears require large strain accommodation between the grains, but the strains can be lowered if the neighboring grains deform with shears of opposite signs [28], as indicated in Fig. 8. Such grain-pairs shears have been recently observed in both hot extruded and hot rolled Al–2Li–0.12Zr alloys [19]. They were detected using a local texture analysis which showed a number of neighboring grains with positive and negative B-shears, as well as individual grains with regions of opposite B-shear. It was determined that the B-shears had been associated with the grains which were originally in the Goss orientation transforming them into Brass. Evidence of similar rotations have been observed by us in the textures of Al–Li binary alloys [10], suggesting that the intensity of the Brass component can be proportional to the extent of B-type relaxed constraint deformation. Such a scenario has been modeled by Hirsch [29] who has quantified the propensity for B-shears by the ratio of the Taylor factors for the full and relaxed constraint deformations. Using such a ratio it was possible to vary the fraction of the grains deforming under the full and relaxed constraints and obtain deformation textures with strong Brass component [29,30]. Since the Taylor factors depend on the type of directional precipitates present in the microstructure [13,31], the development of textures in the hot-rolled ternary Al–Li–Cu alloys can be affected by the precipitates. Additional contribution can come from the solute–dislocation interactions which can promote shear bands compatible with the B-type shears.

Another possible identification of the mechanism that can lead to the development of strong Brass component can come from the analysis of the position of the β-fibers. Fig. 6 shows that this fiber extends from the Brass to the Taylor/Dillamore–Cu position. According to the results from the full (FC) and relaxed constraint (RC) models, this is consistent with the predictions from either combined FC and Sachs models or from the RC model with relaxed B-shears [26,27]. In the former case, the FC model assures the development of a complete β-fiber, while the Sachs model produces maximum intensity only at Brass. Increase in Brass intensity can be achieved by increasing the fraction of grains deforming with one slip system, in concert with the Sachs model. The RC/B-shear model would predict a peak at Brass without the β-fiber. To predict the observed textures, this model also requires that some of the grains deform under FC conditions. As discussed earlier, an increase in the Brass intensity can be in this case obtained by changing the ratio of grains deforming with the FC and RC.

The secondary texture components in the Al–Li–Cu alloys, that is either weak Cube or rotated Cube, can be attributed to small amounts of recrystallization [9,10]. From these two components the Cube is commonly

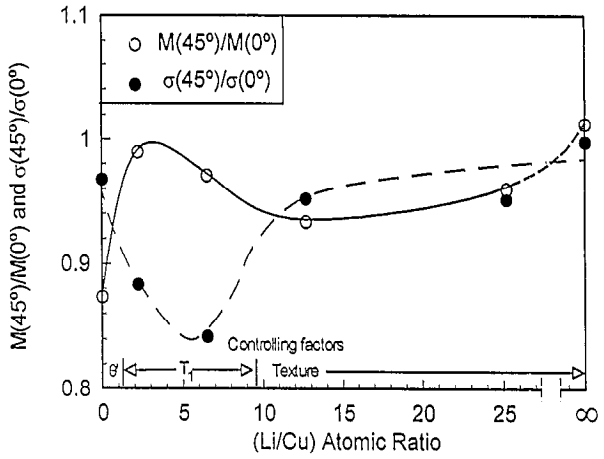

Fig. 9. Effect of the (Li/Cu) ratio on the yield strength anisotropy index, $\sigma(45°)/\sigma(0°)$, and Taylor factor ratios calculated from texture, M(45°)/M(0°), for the hot-rolled and peak aged ternary Al–Li–Cu alloys.

observed during recrystallization of single phase alloys and is expected to be present in all alloys. In the alloys containing second phase dispersions, the particle stimulated nucleation (PSN) for the recrystallized grains can result in the formation of a rotated Cube. This component can be then expected in the alloys which can have either coarse Θ (alloy M) or δ phase (alloys Q and R) present during rolling. However, rotated Cube component was also observed in alloys O and P, Fig. 1, suggesting that these alloys are undergoing some degree of PSN during rolling. Similar textures have been observed by the authors in an identically processed Al–Li binary alloys [10].

The overall development of hot-rolling textures in the Al–Li–Cu alloys can be therefore attributed to the combination of the B-type shears, FC deformation and small amounts of recrystallization. Strong Brass texture is due to the propensity towards B-shears, triggered by the presence of {111} T_1 precipitates and shear banding. The remaining portions of the β-fiber can develop from the grains that deform with five slip systems in accordance with the FC. The development of these textures can be rationalized without references to the non-octahedral slip.

The presence of a strong Brass component in most of the Al–Li–Cu (and Al–Li–Cu–Mg type alloys) has been noted to give rise to the yield strength anisotropy [31,32]. According to FC and RC models, this yield anisotropy leads to a yield strength minimum around 45° with respect to the rolling direction. The anisotropy index describing this effect can be defined in terms of the ratio of $\sigma(45°)/\sigma(0°)$. This has been plotted, as a function of (Li/Cu) ratio, in Fig. 9 for the alloys aged to peak strength. The figure also includes ratios of Taylor factors, M(45°)/M(0°), obtained from ODF texture data and the full constraint model. When texture predominantly affects the yield strength anisotropy, the

trends in both ratios should be similar. This is observed for (Li/Cu) greater than 12, Fig. 9, where the Taylor factor and yield strength ratios are in agreement. For lower (Li/Cu) ratios, the corresponding values are inversely proportional to each other. The possible reason for this discrepancy is the role of directional precipitates on anisotropy. As shown in an earlier publication [32], the {100} habit plane precipitates (as in 2024 alloys) tend to suppress the background texture anisotropy, while {111} precipitates (as in 2090 alloy) reinforce it. In the present alloys, the largest volume fraction of {111} habit plane T_1 precipitates were in the alloys with (Li/Cu) ratios between 2 and 10. These alloys tend to have texture anisotropy amplified by the {111} precipitates, hence their $\sigma(45°)/\sigma(0°)$ ratios are lower than the corresponding M(45°)/M(0°) values. Binary Al–Cu (or 2024 alloys) have {100} Θ' precipitates after aging which tends to suppress the texture induced anisotropy. The anisotropy index in these alloys is therefore smaller than the ratio of Taylor factors. The alloys having (Li/Cu) ratios greater than 12 have significantly smaller volume fractions of the directional matrix precipitates (such as T_1), hence their anisotropy indices and the Taylor factor ratios are similar. The overall yield strength anisotropy of the Al–Li–Cu alloys is then controlled by both texture and directional precipitates, depending on the (Li/Cu) ratio in the alloy composition.

5. Conclusions

- Hot-rolling textures in ternary AL–Li–Cu alloys consist of a complete set of α and β fibers with maximum intensity at Brass.
- The intensity of the Brass component monotonically increases and then decreases with the increasing (Li/Cu) ratio, having a maximum at (Li/Cu) ≈ 6.5. The peak intensity of the Brass component coincides with dominance of T_1 precipitates in the microstructure.
- Because of the presence of Zr in all the ternary Al–Li–Cu alloys they exhibit weak recrystallization texture components either in the form of rotated Cube (high and low (Li/Cu) ratios) or Cube + rotated Cube components (intermediate (Li/Cu) ratios).
- The development of the hot deformation textures can be attributed to the relaxed constraint deformation with B-shears. The shears can be ascribed to the modification of the slip patterns by {111} T_1 matrix precipitates and to the development of shear-bands.
- The maximum yield strength anisotropy in the hot-rolled Al–Li–Cu alloys coincides with maximum intensity of the Brass component. The change in the anisotropy with alloy composition is due to (1) texture in the higher (Li/Cu) alloys and (2) to texture and directional precipitates in the lower (Li/Cu) alloys.

Acknowledgements

The authors are indebted to Mr. J.C. Casato and Mr. E. Llewellyn from Alcoa Technical Center for texture measurements and to Drs. Owen Richmond, J.T. Staley and J. Liu for many stimulating discussions and encouragement. This work was carried out in Alcoa Laboratories (as a part of Alcoa-Navy contract N00019-80-C-0569) prior to AKV's joining ONR. We dedicate this article to Dr. W.G. Fricke, Jr. (passed away on 28 February, 1995) who was instrumental in stimulating our interest in the field of crystallographic texture and yield strength anisotropy.

References

[1] T.H. Sanders, Jr. and E.A. Starke, Jr. (eds.), *Aluminum–Lithium Alloys II*, TMS-AIME, Warrendale, Pennsylvania, 1986.
[2] T.H. Sanders, Jr. and E.A. Starke, Jr. (eds.), *4th Int. Conf. on Aluminum Alloys Their Physical and Mechanical Proterties*, Georgia Inst. of Technology Publication, 1994.
[3] C. Baker, P.J. Gregson, S.J. Harris and C.J. Peel (eds.), *Aluminum–Lithium Alloys III*, The Institute of Metals, London, 1986.
[4] O. Engler and K. Lücke, *Mater. Sci. Eng., A148* (1991) 15.
[5] K. Lücke and O. Engler, *Mater. Sci. Technol., 6* (1990) 1113.
[6] O. Brun, Th. Chauveau, and B. Bacroix, *Mater. Sci. Technol., 7* (1991) 167.
[7] A.W. Bowen, in J.S. Kallend and G. Gottstein (eds.), *Proc. ICOTOM 8*, Metallurgical Society of AIME, Warrendale, PA, 1988, p. 971.
[8] J.R. Hirsch, in T. Chandra (ed.), *Recrystallization '90*, The Minerals, Metals and Materials Society, Warrendale, PA., 1990, p. 759.
[9] J.R. Hirsch, in T.G. Langdon et al. (eds.), *Hot Deformation of Aluminum Alloys*, The Minerals, Metals and Materials Society, Warrendale, PA., 1991, p. 379.
[10] A.K. Vasudevan, M.A. Przystupa and W.G. Fricke, Jr., *Mater. Sci. Eng., 196* (1995) 1.
[11] Academy of Science USSR, *Phase diagrams of Al and Mn*, Nauka, Moscow, 1977, p. 69.
[12] R.J. Roe, *J. Appl. Phys.*, 37 (1966) 2069.
[13] B. Bacroix and J.J. Jonas, in J.S. Kallend and G. Gottstein (eds.), *Proc. ICOTOM 8*, Metallurgical Society of AIME, Warrendale, PA, 1988, p. 403.
[14] A.K. Vasudevan, R.C. Malcolm, W.G. Fricke, Jr. and R.J. Rioja, *Resistance to Fracture, Fatigue and Stress-Corrosion of Al–Cu–Li–Zr Alloys*, Final Report, Contract N00019-80-C-0569, Department of Navy and Alcoa Laboratories, Alcoa Center, PA., 1985.
[15] D.B. Williams and P.R. Howell, in A.K. Vasudevan and R.D. Doherty (eds.), *Aluminum Alloys—Contemporary Research and Applications*, Academic Press, Inc., 1989, p. 365.
[16] W.E. Quist and G.H. Narayanan, in A.K. Vasudevan and R.D. Doherty (eds.), *Aluminum Alloys—Contemporary Research and Applications*, Academic Press, Inc., 1989, p. 219.

[17] E.A. Starke, Jr. and C.P. Blankenship, Jr., in M.G.H. Wells, E.B. Kula and J.H. Beatty (eds.), *Metallic Materials for Lightweight Application*, 40th Proc. of Sagamore Army Mater. Res. Conf., 1993, p. 139.
[18] M.J. Bull and D.J. Lloyd, in C. Baker, P.J. Gregson, S.J. Harris, and C.J. Peel (eds.), *Aluminum–Lithium Alloys III*, The Institute of Metals, London, 1986, p. 402.
[19] J. Mizera and J.H. Driver, in H.J. Bunge (ed.), *Proc. ICOTOM 10*, Trans Tech Publications, *Mater. Sci. Forum*, *157–162* (1994) 1257.
[20] O. Engler, J. Hiesch and K. Lücke, *Acta Metall*, *37* (1989) 2743.
[21] C. Navrotski and B.R. Ward, in T.H. Sanders, Jr. and E.A. Starke, Jr. (eds.), *Aluminum–Lithium Alloys II*, TMS-AIME, Warrendale, PA., 1986, p. 1285.
[22] C. Maurice and J.H. Driver, *Acta Metall*, *41* (1993) 1653.
[23] J.C. Huang and A.J. Ardell, *Acta Metall*, *36* (1988) 2995.
[24] R.L. Fullman, *Trans. AIME*, *197* (1953) 447.
[25] B. Bacroix and J.J. Jonas, *Textures and Microstructures*, *8 & 9* (1988) 267.
[26] J. Hirsch and K. Lücke, *Acta Metall*, *36* (1988) 2863.
[27] J. Hirsch and K. Lücke, *Acta Metall*, *36* (1988) 2883.
[28] E. Aernoudt and P. Stüwe, *Z. Metallkd.*, *61*(H2) (1970) 128.
[29] J. Hirsch, in H.J. Bunge (ed.), *Proc*, *ICOTOM 10*, Trans Tech Publications, *Mater. Sci. Forum*, *157–162* (1994) 1777.
[30] D. Raabe, *Acta Metall Mater*, *43* (1995) 1023.
[31] A.K. Vasudevan, W.G. Fricke, Jr., M. Przystupa and S. Panchanadeeswaran, in J.S. Kannend and G. Gottstein (eds.), *Proc. ICOTOM 8*, Metallurgical Society of AIME, Warrendale, PA, 1988, p. 1071.
[32] M. Przystupa, A.K. Vasudevan and W.G. Fricke, Jr., in J.S. Kallend and G. Gottstein (eds.), *Proc. ICOTOM 8*, Metallurgical Society of AIME, Warrendale, PA, 1988, p. 1051.